

Lift and guidance forces by using iron-magnetic track with side rims interacting with passive HT_C superconducting plate: Experimental analyses

Gino D'Ovidio*, Francesco Crisi, Aurelio Navarra, Giovanni Lanzara

Transportation Department, Faculty of Engineering, University of L'Aquila, 67040, Monteluco di Roio, Italy

Abstract

The paper presents the results of levitation tests carried out by an experimental ring device employing a cooled high critical temperature superconducting ring interacting with magnetic field generated by a circular track with side rims.

The track is composed of toroidal iron structure on which convex surface three homopolar ring sets of permanent magnets (PM) are arranged to exalt the flux density in the top side of track.

The experimental device is conceived and constructed to reproduce, by analogy, the static and dynamic behaviour of a passive superconducting “runner” of levitated vehicle riding above the magnetic guideway.

In a wide range of work conditions, lift and guidance performances of system have been tested.

Moreover, a two-dimensional finite element parametric model of experimental device has allowed carrying out several numerical analyses.

© 2006 Elsevier B.V. All rights reserved.

Keywords: Magnetic levitation; High critical temperature superconductor; Permanent magnet

1. Introduction

At University of L'Aquila a research program on applying high critical temperature superconductor (HT_CS) materials to practical transportation applications is developing.

The aim of the research program is to prove deeply the concept of a Maglev vehicle based on HT_CS levitation and guidance, by means of methodological, both numerical and experimental, analyses.

Compared with other maglev systems, the vehicle using HT_CS is stable lifted over magnetic guideway thanks to the use of YBCO (Yttrium–Barium–Copper Oxide) bulk superconductors type that operate at liquid nitrogen temperature. The guideway consists of two parallel permanent magnetic tracks; each one generates magnetic flux density on top side. The bulks HT_CS constitute the superconducting “runners” of vehicle that interact the magnetic field over the centers of each track so that levitation forces can be generated between way and vehicle.

Previously several numerical analyses on interaction forces between HT_CS and the magnetic field have verified that the entity

of forces is widely compatible with transportation applications [1–2].

Successively experimental ring model device reproduced, by analogy, the behavior of Maglev vehicle, with superconducting “runners”, riding on magnetic guideway, has been designed and constructed. Instead of achieving a linear machine of finite dimension, a circular way (primary) interacting with a HT_CS ring (secondary) have been already designed and manufactured.

Moreover, levitation and propulsion tests have been already carried out by means of an experimental model device employing the same HT_CS ring interacting with different typologies of circular magnetic tracks and consisting of:

1. Windings three-phase voltage fed [2–3].
2. Permanent magnets (PM) arranged in Halbach Array [4].
3. Iron-homopolar PM [5–6].

This article summarises the results of levitation performance of a system utilising a further magnetic track consisting of the iron-homopolar PM with side rims.

The main components of the magnetic track derive from a preliminary numerical design focused on the maximization of the magnetic flux on guideway topside; this specific work phase is not described in this report.

* Corresponding author. Tel.: +39 0862 434 106; fax: +39 0862 434 143.
E-mail address: dovidio@dau.ing.univaq.it (G. D'Ovidio).

Table 1
Main data of YBCO ring

| | |
|---|----------------------|
| Outer diameter (mm) | 435.0 |
| Average diameter (mm) | 393.2 |
| Inner diameter (mm) | 353.2 |
| Thickness (mm) | 11 |
| Trapped field (T (77 K)) | >1 |
| Critical current density (A/cm ² (77 K, self field)) | >8 × 10 ⁴ |

Section 2 of this article begins with an illustration of experimental model device and a brief review of the main technological and magnetic characteristics. Section 3 reports the field measurements and discusses the results of the experimental tests in terms of levitation forces. Many of the key results are in Section 4, where the numerical analyses are presented and the outcome discussed. The concluding remarks are in Section 5.

2. Experimental device

The experimental model device consists of two main components that do not have physical contact:

2.1. Superconducting secondary

HTcS ring constituted by close array of 34 YBCO monoliths trapezoidal shaped properly fitted, by two rings of austenitic stainless steel—non magnetic alloy AISI 304—on the bottom of the circular vessel, filled with liquid nitrogen (77 K).

Table 1 contains the main data of YBCO ring.

As well known, superconductors are materials capable, at temperature near absolute zero, to conduct electricity with zero resistance and as well as become strongly diamagnetic [7–8].

The YBCO is a ceramic composition based on copper oxide belonging to type II superconductor. Type II superconductor presents a partial “Meissner” effect in which a superconductor excludes magnetic flux [9].

Fig. 1 shows the YBCO ring; Fig. 2 shows the austenitic stainless steel device fixing the set of 34 YBCO monoliths.

2.2. Primary track

Iron-magnetic circular inductor consisting of iron toroidal structure with a “U” shaped generator section with PM. More in detail the iron structure working

Table 2
Main data of inductor

| | Horizontal | Outer side rim | Inner side rim |
|------------------------------|--------------------------|-------------------------|-------------------------|
| Iron structure | | | |
| Outer diameter (mm) | 523.2 | 523.2 | 279.2 |
| Average diameter (mm) | 393.2 | 515.2 | 271.2 |
| Inner diameter (mm) | 263.2 | 507.2 | 263.2 |
| Thickness (mm) | 12 | 8 | 8 |
| Height (mm) | 130 | 94 | 94 |
| | Z magnetisation axis | Y magnetisation axis | Y magnetisation axis |
| Permanent magnet ring | | | |
| Number of PM | 10 | 40 | 20 |
| Outer diameter (mm) | 433.2 | 513.2 | 289.2 |
| Average diameter (mm) | 393.2 | 505.2 | 281.2 |
| Inner diameter (mm) | 353.2 | 497.2 | 273.2 |
| Width (mm) | 40 | 8 | 8 |
| Height (mm) | 25 | 25 | 25 |
| Volume (mm ³) | 1235.3 × 10 ³ | 317.4 × 10 ³ | 176.7 × 10 ³ |



Fig. 1. YBCO ring.

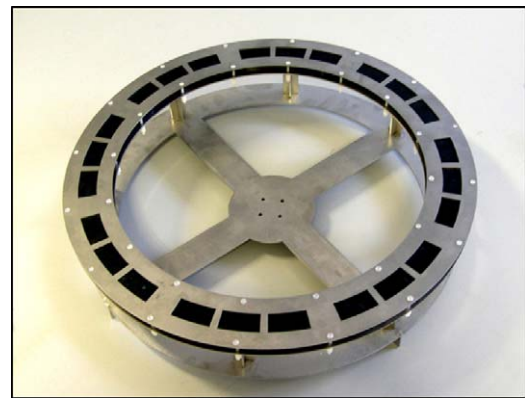


Fig. 2. YBCO ring with fixing device.

as flux collector, is composed by a horizontal surface with two vertical lateral sides. Three sets of homopolar Nd–Fe–B (Neodymium–Ferrum–Boron) PM are mounted on iron structure according the following configuration:

- One set of circle sectors of PM, magnetized according the (Z) vertical axis, is fixed on middle crown of the horizontal surface of disk.
- Two sets of homopolar circle sectors of PM, magnetized according the (Y) radial axis, are fixed respectively, on vertical surface of inner and outer lateral sides.

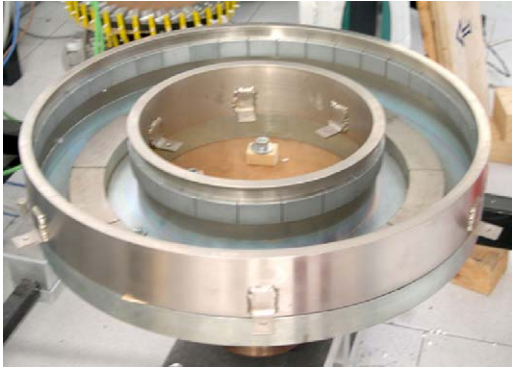


Fig. 3. Circular magnetic track.



Fig. 4. Detail of side rims of magnetic track.

Table 2 contains the main data of the circular iron-magnetic track.

Figs. 3 and 4 show respectively, the overall view of circular magnetic track and its detail.

The main characteristics of utilised Nd–Fe–B PM [10–11] are:

- Residual induction (B_r) = 1.2 T.
- Coercitivity (H_C) = 892 kA/m.
- Maximum energy product $(B \times H)_{\max} = 279 \text{ kJ/m}^3$.

The YBCO ring is mounted above the circular track that can mechanically rotate around its vertical axis.

The rotational speed of primary is controlled by a driving belt coupled to ac motor fed with three-phase inverter; in this way, the module versus the rotational speed can be controlled in order to reproduce several operating conditions.

A hydraulic jack, jointed to precision mechanical device, permits to vary the air-gap between primary and secondary; the operative gap is reduced because of bottom wall thickness (2 mm) of cryogenic vessels.

The interaction forces are evaluated on the secondary by a measurement system consisting of bi-axial sensor measuring levitation force (F_z) and torque (M).

Fig. 5 shows the overall view of the experimental ring device.

Compared to the maglev vehicle riding along the magnetic way, this experimental device realizes the following analogies:

- Circular inductor simulates the magnetic guideway with infinite length.
- HTcS ring simulates the superconducting “runner” of vehicle.
- Relative motion between vehicle and guideway is obtained by imposing mechanical rotation of circular track around its vertical shaft and by locking the secondary.

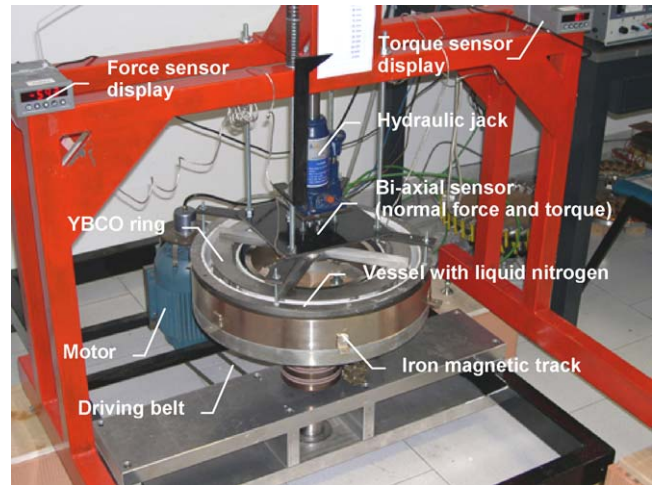


Fig. 5. Overall view of experimental ring model device.

3. Tests

Several experimental tests have been carried out in order to characterise the model device and to measure the levitation and drag forces varying rotational speed and air-gap length.

The tests were articulated into two phases focused on measurements of:

- magnetic field of inductor;
- lift and drag forces.

3.1. Magnetic field measurement

Firstly the magnetic field of the proposed magnetic track has been tested and mapped.

More in detail the air-gap flux density distribution was measured by means of a Hall probe positioned at different height (H) from the surface of magnetic track.

Fig. 6 shows the transverse distribution of magnetic field of a track with reference to a system configuration with locked primary (0 rpm).

Particularly Fig. 6a shows the vectorial representation of (B) flux density distribution with reference to the radial cross section of circular track.

The figure shows that the flux density is strictly contained into the convex surface of the track.

Fig. 6b shows the maximum values of (B_x) horizontal component flux density versus radial offset (ΔY).

The figure points out that B_x configuration has an emi-symmetric distribution that allows achieving a strong guidance force.

Fig. 6c shows the maximum values of (B_z) normal component of flux density versus offset (ΔY). The figure points out that B_z has a symmetric distribution with maximum value (0.4 T) at 0 offset and $H = 0$ mm.

In correspondence of a combination of high values of offset and H , the magnetic track produces negative B_z : this phenomenon is evident in the air nearest the side rims.

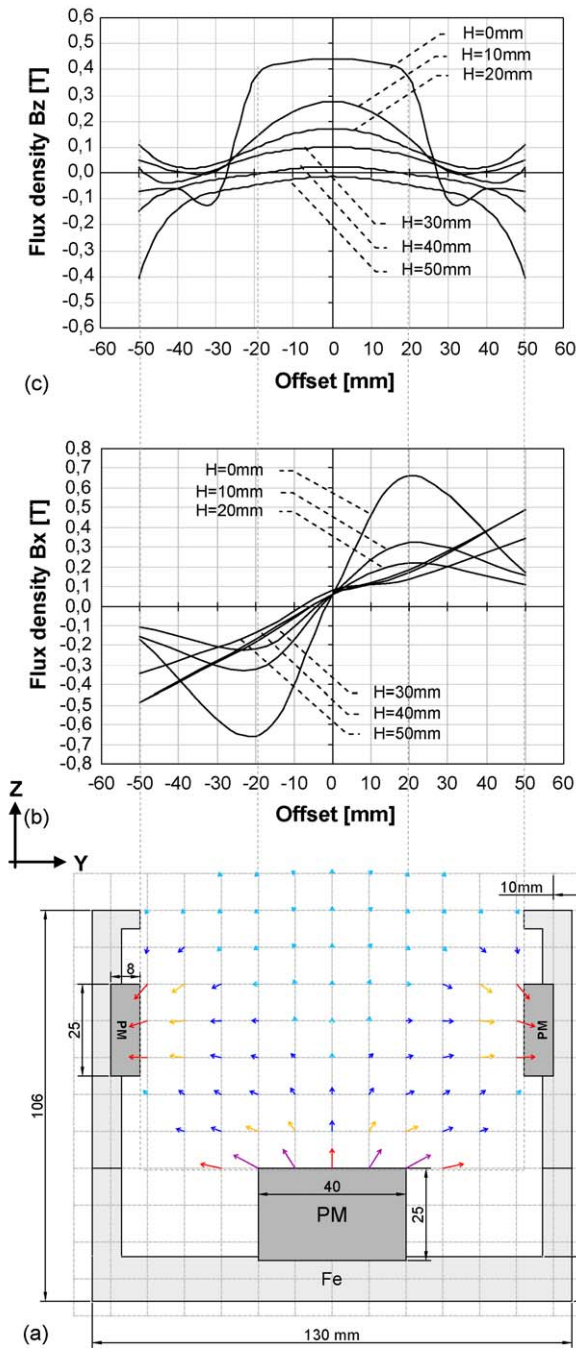


Fig. 6. Transverse distribution of magnetic field (B) of the circular track: (a) B vectorial representation; (b) B_x component; (c) B_z component.

Fig. 7 shows the distribution of magnetic field of the track along the vertical direction at 0 offset.

The result of field characterisation demonstrates that both magnetic field intensity and gradient are achieved.

3.2. Levitation tests

A series of levitation tests has been carried out by means of the above experimental device, varying some parameters of system as the air-gap length (H_T) and the rotational speed (rpm). The YBCO ring has been cooled in a zero magnetic field with liquid

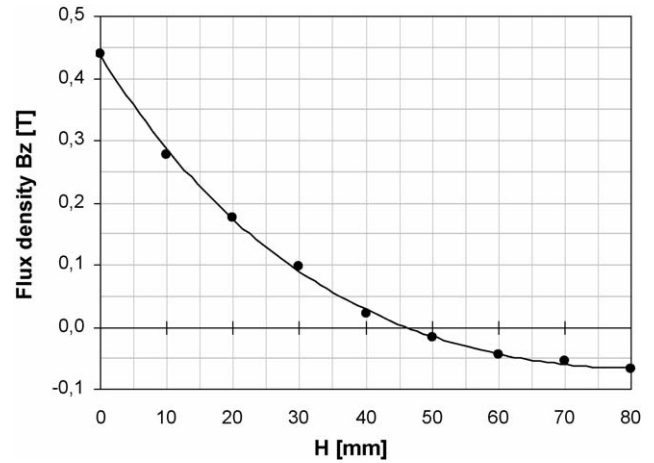


Fig. 7. Distribution of magnetic field of the track along the vertical direction at 0 offset.

nitrogen and then was positioned above the magnetic track. The displacement of a HTCS ring above the inductor causes inductive currents and therefore lift forces for all rotational speed. It is well known that the forces between the superconductor and the guideway are directly proportional to the field entity and the field gradient. The tests were conducted at different air-gap lengths (H_T) until a rotational speed of 500 rpm that correspond to 10.3 m/s.

To compare the levitation results to ones obtained by other system configuration [5–7], the levitation pressure (P_Z) quantity has been introduced:

$$P_Z = \frac{F_Z}{S_R}$$

with: F_Z =lift force; S_R =induced YBCO ring surface (493.7 cm^2).

Fig. 8 shows the lift pressure versus rotational speed for different air-gap lengths (H_T). It is evident how the levitation pressure keeps constant at all speed value; obviously it decreases as air-gap-lengths rise.

The obtained results demonstrate that the levitation force do not depend on the relative speed between primary and secondary;

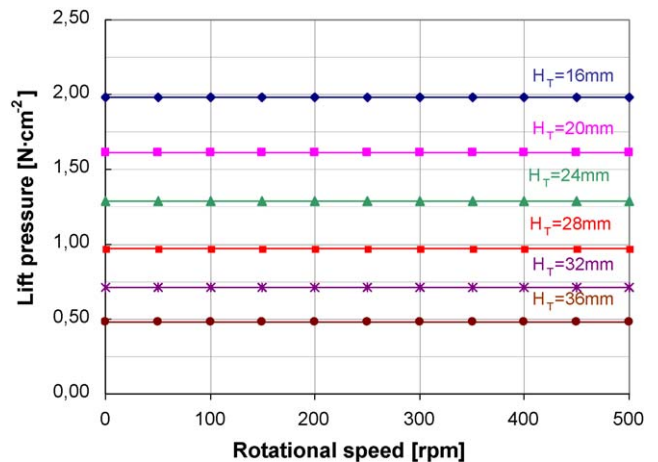


Fig. 8. Lift force vs. rotational speed at different air-gap length (H_T).

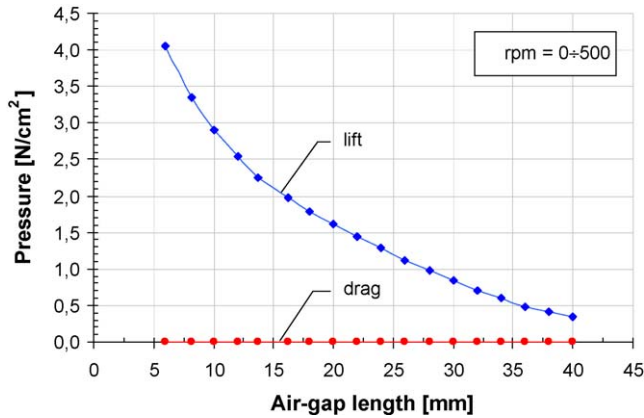


Fig. 9. Lift and drag forces vs. air-gap length at range of 0–500 rpm.

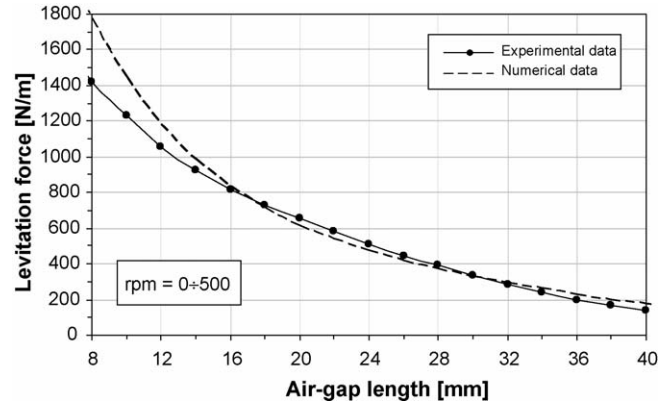


Fig. 10. Comparison between numerical and experimental data.

the system operates with a large air-gap and no feedback control for stable levitation is required.

Moreover, the measurements carried out by the torque sensor show that the magnetic resistance (drag force) is completely absent at every speed values.

The entity of drag force (F_X) is obtained by dividing the measured torque value (M) by the average radius (0.1966 m) of HTcS ring. Consequently the (P_X) drag pressure quantity is so defined: $P_X = F_X/S_R$

The results assume a significant interest in relation to Maglev application because they demonstrate that the proposed system eliminates completely the magnetic resistance that characterises the functioning of others current transportation systems.

Fig. 9 shows the levitation and drag forces versus air-gap length at range of 0–500 rpm; the values of lift force rises according to exponential trend as air-gap length decrease.

4. Numerical analyses

To investigate deeply the lift and guidance forces, a bi-dimensional element finite parametric model of experimental equipment, described in Section 2, has been carried out.

The model has been approached by using several variables that make it possible to analyze the role that each variable assumes within the economy of the system in terms of performance.

The model analyses the phenomenon on Z–Y plan evaluating lift (F_Z) and guidance (F_Y) forces.

Rare-earth magnets ($B_r = 1, 2 \text{ T}$, $H_C = -900 \text{ kA/m}$, $\mu_r = 1$) and non-linear B–H characteristics for the massive iron were taken into account [10–11].

The model has been tuned starting from the experimental results of the previous tests.

The good agreement between numerical and experimental results was obtained taking into account a low electrical resistivity ($10^{-10} \Omega\text{m}$), relative permeability value equal to 1 and relative speeds of $V_Z = -0.015 \text{ m/s}$, $V_Y = 0$ for modelling the HTcS material. Fig. 10 shows the comparison of numerical and experimental values of levitation force versus air-gap length at 0–500 rpm.

A previous numerical analysis has allowed evaluating the gain, in terms of lift force, obtained by the interaction of the same superconductor with two types of inductor: a track with iron-magnetic side and a track without the PM on iron side rims.

To compare the levitation performance of two system configurations, the results of tests have been normalized in relation to the same volume of PM displaced on both inductors: in other terms, for both inductors, the levitation force has been evaluated with equal volume of PM.

Fig. 11 shows the lift forces gain (%), versus air-gap length obtained utilizing the track with iron-magnetic side rims in relation to track without PM on iron side rims. Figure points out that there is lift gain at all air-gap length; particularly the lift gain is about 45% at air-gap of 37 mm.

Figs. 12 and 13 show respectively, a 2D and 3D view of magnetic flux distribution obtained by means of the numerical model.

Particularly Fig. 12 emphasizes the flux line distribution in the cross section of track; Fig. 12a and b are particularly referred to a system configuration without and with the presence of superconducting plate.

It is evident how the presence of PM arranged on side rims emphasizes the magnetic field in air summing own contributes to

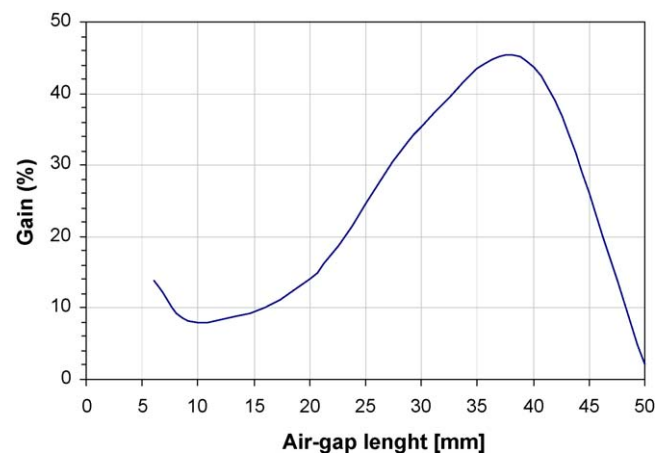


Fig. 11. Lift force gain vs. air-gap length.

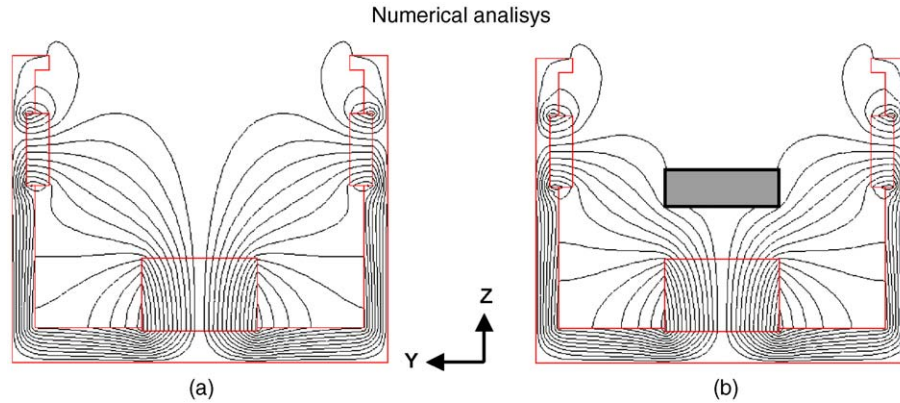


Fig. 12. Flux line distribution in a cross section of device: (a) track without superconducting plate; (b) track with superconducting plate at air-gap of 20 mm.

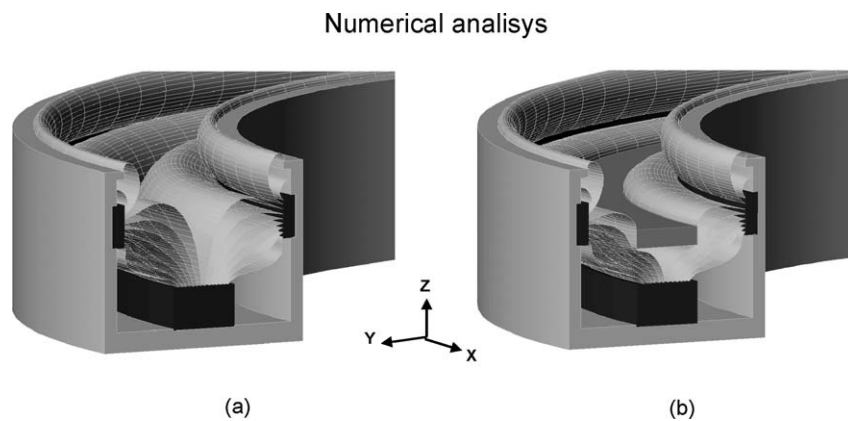


Fig. 13. Three dimensional views of field configuration: (a) track without superconducting plate; (b) track with presence of superconducting plate at air-gap of 20 mm.

horizontal PM one. This particular configuration of flux density allows increasing the magnetic interaction with superconductor at significant air-gap. In analogy, the system permits to maglev vehicle to work with a significant operative height from the track within the correlating advantages.

Moreover, the flux density generated by the vertical magnets arranged on side rims contribute to increase considerably the (B_x) component that, interacting with superconducting plate, allows centring it on the track.

Fig. 13 points out the three-dimensional views of flux line distribution in the cross section of track. Fig. 13a show the configuration of magnetic field generated by the track. Fig. 13b is referred to a system configuration with the presence of superconducting plate; it emphasizes, with relation to Fig. 13a, how the superconductor, at air-gap of 20 mm, interacts with magnetic flux lines comprising and deforming them.

Figures show that the track generates a magnetic field having a field gradient perpendicular (Z) and homogeneous behaviour along the annular direction according to motion one (X).

However, the results of numerical analysis confirm that flux lines are strictly bounded on the space defined by the concave iron structure of the track.

Lift and guidance forces have been carried varying the offset (ΔY) and the air-gap length (H_T). The forces are evaluated in

relation to one linear meter of the magnetic track and they are expressed accordingly in Newton per meter (N/m).

Fig. 14 shows both the lift (F_z) and guidance (F_y) forces versus offset (ΔY) at four values of air-gap lengths (H_T). The guidance (lateral) force depends on both trapped flux in the superconductors and repulsive action on it generated by lateral PM.

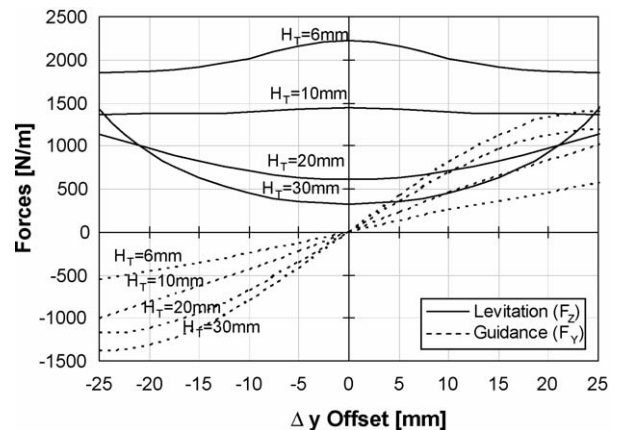


Fig. 14. Track with side rims: lift and guidance forces vs. offset (ΔY) at four air-gap lengths (H_T).

The analysis of the Figure evidences:

1. In correspondence of 0 offset, the superconductor is perfectly centered on the track and the system produces the following forces:
 - F_Y is null;
 - F_Z is maximum at low values of H_T (6–10 mm); vice versa F_Z is minimum at a big values of H_T (20–30 mm).
2. In correspondence of ± 25 mm, the superconductor has a maximum offset on the track and the force are:
 - F_Y is maximum;
 - F_Z is minimum at low values of H_T (6–10 mm); vice versa F_Z is maximum at a big values of H_T (20–30 mm).

The result emphasizes that the system produces both stable lift and guidance force at all offset.

5. Conclusion

Levitation performances of circular magnetic tracks with side rims, interacting with high critical temperature superconducting ring have been analysed and tested.

The track emphasizes magnetic flux density on top side and produces a magnetic field having a perpendicular (Z) gradient and homogeneous behaviour along the radial direction according to motion one (X).

However, the flux lines are strictly bounded on the space defined by the concave iron structure of the track.

The results of tests have pointed out that the levitation force do not depend on relative speed between magnetic track and superconductor.

Moreover, the system do not produces magnetic resistance to the motion and achieves both stable lift and guidance force at all offset.

The proposed track with iron-side rims, compared to one that has only iron side rims, allows obtaining lift gain at all air-gap length.

These results are useful to design high performance Maglev vehicle with HTCS on board interacting with a guideway composed of iron and PM.

References

- [1] G. Lanzara, G. D'Ovidio, C. Masciovecchio, M. Villani, Superconducting sheets for train support and traction: finite element analysis, in: Proceedings of the Second International Symposium on Linear Drives for Industry Applications (LDIA), Tokyo, Japan, 8–10 April 1998.
- [2] G. D'Ovidio, M. Villani, F. Crisi, S. Monaco, A. Navarra, G. Lanzara, 3D finite element analysis of inductor «way» and inclined multi-sheets type secondary, in: Proceedings of the Eighth International Conference on Computer Aided Design, Manufacture and Operation in the Railway and Other Advanced Mass Transit Systems (COMPRAIL), Lemnos, Greece, 12–14 June 2002.
- [3] G. D'Ovidio, F. Crisi, A. Navarra, G. Lanzara, Magnetic levitation by high superconductor plate short secondary interacting with traslating field: experiences, measurements and modelling, J. Mater. Processing Technol. 161 (1–2) (2005) 45–51, Elsevier Edr.
- [4] G. D'Ovidio, G. Lanzara, F. Crisi, A. Navarra, Electrodynamic interaction between HTSC plate short secondary and way with permanent magnet arranged in halbach arrays, in: Proceedings of the Third International Symposium on Linear Drives for Industry Applications (LDIA), Birmingham, United Kingdom, September 2003.
- [5] G. D'Ovidio, F. Crisi, A. Navarra, G. Lanzara, Levitation by passive high temperature superconducting plate and iron-magnetic track: tests and numerical analyses, in: Proceedings of the Ninth International Conference on Computer Aided Design, Manufacture and Operation in the Railway and Other Advanced Transit Systems (COMPRAIL), Dresden, Germany, May 2004.
- [6] G. D'Ovidio, F. Crisi, A. Navarra, G. Lanzara, Experimental Ring Model Device with Bulk HTSC “Runner” and Magnetic Guideway: Maglev Tests and Numerical Analyses, in: Proceedings of the Eighteenth International Conference on Magnetically Levitated Systems and Linear Drives (MAGLEV), Shanghai, China, 26–28 October 2004.
- [7] C.P. Poole, T. Datta, H.A. Farach, Copper Oxide Superconductors, John Wiley and Sons, 1988.
- [8] T. Matsushita, P.J. Lee, S. Ochiai, Composite Superconductors, M. Dekker. Inc., New York, 1994.
- [9] D. Shi, et al., High-temperature Superconducting Materials Science and Technology, Pergamon, Trowbridge, 1995.
- [10] H.E. Knoepfel, Magnetic Fields, John Wiley & Sons, Inc., New York, 2000.
- [11] J.F. Gieras, M. Wing, Permanent magnet motor technology, in: Design and Applications, Marcel Dekker, Inc., New York, 1997.